

**DETAILED RESPONSE TO REVIEWERS' COMMENTS**

We thank all the reviewers, and the editor, for their thorough and detailed comments, as well as their interest in our work. These comments have helped us improve our manuscript significantly.

We sincerely appreciate the opportunity to resubmit our manuscript for consideration. Below you will find our point-by-point response to the reviewers with summaries of changes corresponding to the revised and resubmitted manuscript. We hope that this new version addresses all concerns and better meets the journal standards.

In particular, we have proceeded to a new selection of the events that we consider in our analysis. Following the questions by the reviewers, we decided to be more selective than in a previous version of the paper. In addition to the better presentation of the data suggested by one of the reviewers, we believe this strengthens our message and our analysis.

Below are our detailed responses to the specific comments raised. All comments related to manuscript lines in the present letter, refer to the revised version of our work. Paragraphs in dark green represent comments added to the revised version of the manuscript, while those in blue have been included in the Supporting Information.

---

**REVIEWER A:** *The work of Jara and collaborator present interesting evidences of slow slip occurrence along the northern Chile – Peru region, detected with an innovative method. The results are convincing, and are supported by different tests which help the reader to be confident in the final observables. The authors also estimated coupling, and about this point I strongly disagree with them. I cannot understand the concept of coupling estimated for a fault which slip episodically. Unless one use data spanning exactly the same time period for coupling estimation and slow slip detection, I do not see how it is possible to compare the two results (see my detailed comments).*

*But this is a long debate, and this last point does not weaken the results of the work from Jara et al., which should be accepted for publication after very minor reviews.*

*I proposed a list of potential citation, which mostly include my works (the ones I know the best), but the authors can for sure find some more relevant articles to corroborate the results and inform the reader.*

*Please find below some more detailed comments about the article:*

Dear Pr. Poli, we appreciate the kind comments pointing out the importance of our work. In the following lines, we discuss the statement about SSE and coupling, as well as include the reviewer's suggested

reference to improve the manuscript.

**REVIEWER A:** 1) *In the introduction you mention the widespread observations of slow slip events in a large variety of faults. You might want to support this point with some evidence of slow slips in normal faults:*

*Gualandi, Adriano, et al. "Aseismic deformation associated with an earthquake swarm in the northern Apennines (Italy)." Geophysical Research Letters 44.15 (2017): 7706-7714.*

*Cheloni, Daniele, et al. "Aseismic transient during the 2010–2014 seismic swarm: evidence for longer recurrence of  $M \geq 6.5$  earthquakes in the Pollino gap (Southern Italy)?" Scientific reports 7.1 (2017): 576.*

*This is for sure not a comprehensive list of articles.*

*Interestingly, some high-resolution seismological observations we made on the Alto Tiberina normal fault, seems to point towards an imbricated slip behavior, similar to the burst-like one discussed in 59-67.*

*Essing, David, and Piero Poli. "Spatiotemporal Evolution of the Seismicity in the Alto Tiberina Fault System Revealed by a High-Resolution Template Matching Catalog." Journal of Geophysical Research: Solid Earth 127.10 (2022): e2022JB024845.*

*However, I understand that adding all this to the introduction might make the manuscript's introduction a little to 'heavy'.*

We added the articles about the Alto Tiberina and Pollino fault systems in Italy, as suggested by the reviewer (Lines 95-96).

**REVIEWER A:** 2) *From line 102 you discuss the observation of GNSS velocity change (or decoupling) following large earthquakes. Similar observations have been done along the Chilean subduction after several large events. You may want (or not) to discuss this works:*

*Ruiz, Sergio, et al. "The seismic sequence of the 16 September 2015 Mw 8.3 Illapel, Chile, earthquake." Seismological Research Letters 87.4 (2016): 789-799.*

*Ruiz, S., et al. "Reawakening of large earthquakes in south central Chile: The 2016 Mw 7.6 Chiloé event." Geophysical Research Letters 44.13 (2017): 6633-6640.*

*Melnick, Daniel, et al. "The super-interseismic phase of the megathrust earthquake cycle in Chile." Geophysical Research Letters 44.2 (2017): 784-791.*

We added references to the proposed articles, emphasizing that observations post-Maule earthquake are of longer wavelength than those following the Tarapaca earthquake. The main text has been modified as follows (Lines 136-140):

Comparable changes in surface velocity field, observed following the 2010 Maule earthquake, have also been observed in the regions affected by the 2015 Illapel (Ruiz et al., 2016) and 2016 Chiloé (Ruiz et al., 2017; Melnick et al., 2017) earthquakes. Such shifts in surface velocity may be linked to postseismic viscoelastic processes acting over long distances (Bouchon et al., 2018) in contrast to the localized behavior observed after the Tarapaca earthquake (Jara et al., 2017).

**REVIEWER A:** 3) *About coupling estimation: You use a variety of measurements, spanning variable time ranges, to estimate coupling along the subduction interface. At the same time, you suggest the existence of many slow slip events. Does it make sense to talk about coupling? If we consider a single GNSS time series, spanning a period  $T_1$  without slow slips, it will provide a coupling value, much different from a one on a period  $T_2$  which include several slow slips. For example, in line 189 you mention how the megathrust is decoupled at depth, but it is also (temporally) decoupled in the shallower part, how this modify your coupling map? Can you also please provide a more detailed list of time period used to estimate the coupling, and discuss in more details how the slow slips occurrence does modify this coupling map?*

We now include the time scale of observation periods for the GNSS measurements used (lines 204-206). InSAR observations were already described in the manuscript (line 207). Additionally, we provide a detailed description of how we estimate probability distribution functions for coupling and our slow events in the Supporting Information of this manuscript (see also the detailed response to reviewer 2 on this topic).

Regarding Pr. Poli's suggested discussion on coupling, we believe coupling should be understood as the mean kinematic locking state over a period considered as interseismic. When it is possible to detect and correct for large slow slip events, then one should do so. However, here, we detect small events which should be considered as fluctuations around this mean. We now include a paragraph discussing this idea (lines 407 - 424).

**REVIEWER A:** 4) *From line 238, when you describe the stacking procedure, the text becomes a little complicated to follow. I think it would be helpful to graphically show this process or at least some results, perhaps in fig. S31. Or perhaps here refer to the figure S33 where some of the stacks are visible.*

We appreciate Pr. Poli's valuable comment, which has assisted in clarifying the methodology presented in this article. Figure S31 (Supporting Material) has been revised to feature a synthetic example illustrating the method accompanied by a comparison with a correlation that includes a common mode. In Figure S31b, the panel shows the comparison between the correlation function at the AEDA station (with the largest displacement) and the cumulative sum of all stations. This figure highlights the importance of

using all stations when applying GNSS stacking to extract the signal from geodetic noise. A corresponding comment has been included in the main text, specifically in lines 274-289.

**REVIEWER A:** 5) Section 2.5: Line 286: *Why did you choose a duration of 40 days? Few lines after you mention that you ‘evaluate the duration of magnitude and duration’, can you please provide more insights about how this is done? Still on this duration point, you mention (line 294) that the duration range from 9 to 40 days, is the latter value influenced by your previous choices? How? In figure 5, the comparison of the time evolution of the stacked signal (5a-d) should be accompanied by the time and magnitude of the seismicity in the same period. I suggest this kind of analysis for each of the detected slow slip, to understand their relationship with seismicity (if any). For example, is the seismicity mostly swarm-like? Are some slow slips post- seismic transients of small events, which escaped the trajectory model (you correct for post-seismic signal just if  $M_w$  is larger than 7.5, and imposing a function which might differ from the real post-seismic time evolution).*

We set the template duration, opting for 40 days with a specific rationale. As highlighted by Rousset et al. (2017), shorter templates (10-20 days) lack the clarity seen in a 30-day template and correlation peaks do not clearly emerge in synthetic examples. Following the idea proposed by Rousset et al. (2017), we test various durations, including 40 days (Figure RB1). Our results show that a 40-day template effectively eliminates certain spurious correlation peaks observed with a 30-day template, enhancing the visibility of correlation peaks in the geodetic noise during synthetic events. Based on this observation, we opted for a 40-day template. We now include the following figures in the Supporting Information (Figures S58-S59), and a comment at Lines 329-331.

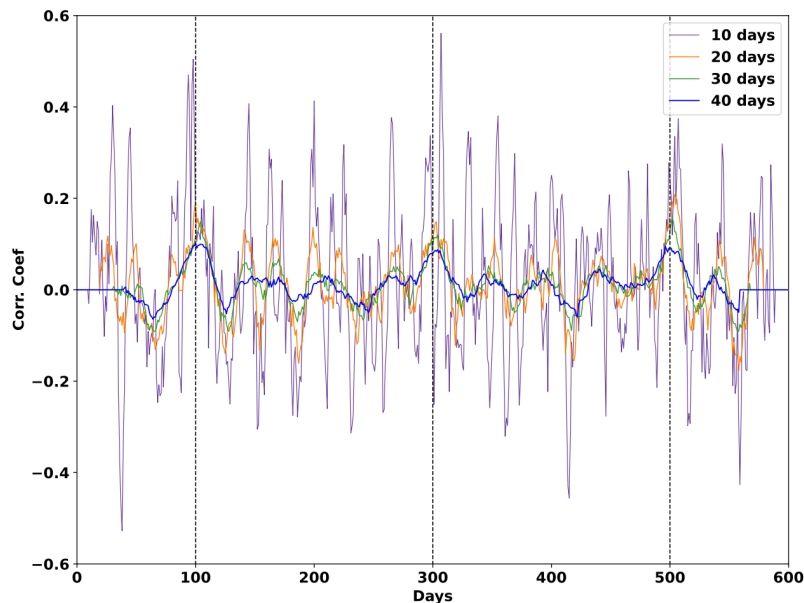


Figure RB1: Correlation functions for various template durations: 10 (purple), 20 (orange), 30 (green), and 40 (blue) days. Vertical dashed lines indicate the center time of a synthetic slip event equivalent to a magnitude of  $M_w$  6.0 and durations of 10 (day 100), 20 (day 300), and 30 (day 500) days. The tested patch location aligns with Figure S31.

We assess the duration and magnitude of our events by fitting Eq. 5 from the main manuscript, along

with two linear regressions featuring constant velocity (see Lines 284-287). In Eq. 5, we estimate the duration and slip amplitude, which is then converted to moment magnitude ( $M_w$ ). Pr. Poli rightly points out that the choice of our template impacts event selection. We only consider detections with a duration of  $T \leq 40$  days. This is illustrated in Figure RB2, comparable to Figure RB1, with synthetic events lasting 60 (a), 80 (b), and 100 (c) days, centered on day 150 (Figure S59, Supporting Information). Across template durations (10, 20, 30, or 40 days), no correlation peaks are observed in the correlation function. Consequently, we deem events valid only if their duration is  $T \leq 40$ .

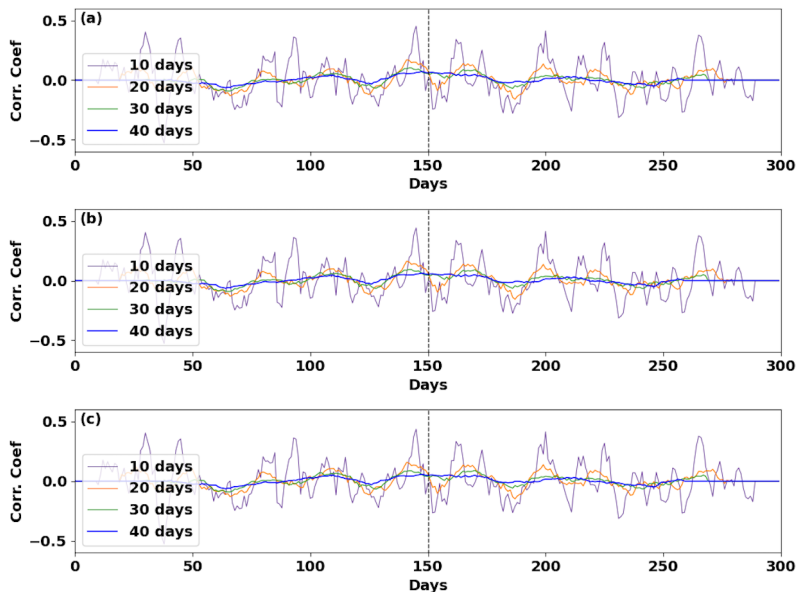


Figure RB2: Same caption as Figure RB1, but with synthetic events lasting for 60 (a), 80 (b), and 100 (c) days centered on day 150.

Figure 5 does not include seismicity in panels a and e to avoid overloading the figure. Seismicity, scaled by magnitude and colored by date, is plotted in panels d for Event #12 and h for Event #7, as per Reviewer B’s request (updated accordingly). The analysis of seismicity and the estimation of the seismic/aseismic ratio are detailed in the supplementary material and the last column of Table S43.

The definition of swarms in the zone has been discussed by Jara et al. (2017) (Supporting Information). At least two swarms are identified, but they do not correlate with the occurrence of our detected slow events. Regarding postseismic transients, two events seem related to this phenomenon. Event #7 appears to be an aseismic pulse after the 2014 Iquique earthquake (Lines 464 - 468). We acknowledge Pr. Poli’s comment, and agree that our trajectory model cannot detect transient pulses departing from the logarithmic function used for the postseismic slip estimation of both earthquakes. Event #12 occurs during the preparation phase of the Iquique earthquake, a finding consistent with tiltmeter data in the zone (Boudin et al., 2021) (Lines 472 - 482). Therefore, based on the seismic/aseismic ratio analysis, we conclude that the remaining events are interseismic transients.

**REVIEWER A:** 6) Line 332: You reason around the work of Gomberg et al., (2016), but not all the

*readers will be confident with their approach. Can you please clarify a bit more how you infer the rupture velocity and stress drop? Please also state more clearly that the rupture you observe is crack-like because of the 1/3 scaling. However, I am not confident about your ability to resolve any scaling given the small range of moment you resolve, together with the errors in size and duration that might affect your data.*

In agreement with both Pr. Poli and Pr. Freymueller (Reviewer B), we now provide a detailed step-by-step description of our procedure for this particular point. This information is available in our comprehensive response to Reviewer B and in the Supporting Information of our article.

**REVIEWER A:** 7) *Line 338: I go now back to point 3 of my review. You here claim what I was mentioning above: the coupling is an average, then you should let the reader understand over which period is the average. Can you please provide the time period of the data used for i) coupling estimate and ii) slow slips search? Still on this point, I think is hard to compare the coupling map with slow slip, unless a clear view of the data used is presented. If some data are removed (added) to the analysis in some particular zone of the study area, and this data were (or were not) recorded during slow slip events, the coupling estimate would change. Then, if this is the case, I do not see how the coupling map can be related with the slow slip positions.*

We have already answered this question above. It is essential to reiterate that interseismic coupling represents an average, and our events reflect fluctuations around this average.

**REVIEWER A:** 8) *In line 379 you discuss the role of ‘complexity’ which was argued to play an important role in modulating the release of stress also in our work: Poli, Piero, Andrei Maksymowicz, and Sergio Ruiz. “The Mw 8.3 Illapel earthquake (Chile): Preseismic and postseismic activity associated with hydrated slab structures.” *Geology* 45.3 (2017): 247-250.*

We have added the reference accordingly on Line 459.

**REVIEWER A:** 9) *In my last comment, I (strongly) suggest to clarify in the discussion this ‘issue’ about coupling and provide more insights to better quantify the coupling values at the positions of the slow slip events.*

We now discuss this question in the manuscript (lines 407 - 424). Additionally, our manuscript now includes a detailed explanation of how coupling relates to the location of our detected events (Supporting Information).

---

**REVIEWER B:** *This paper presents a new approach to detect small slow slip events along the southern*

*Peru-northern Chile subduction zone. The authors use template matching to identify the signatures of small slow slip events.*

*I think a more clear presentation of the events and data is needed in the main paper, at least for the most clearly recorded events. The key question I still have after reading the paper is whether or not the authors are really extracting signal from the noise, and how certain are their estimates of the events' properties? I think the presentation of the extraction of the events from the data can be improved. I have some other concerns that relate to the uncertainties of some derived quantities, and the resulting interpretations.*

Dear Pr. Freymueller, your questions and comments have helped us improve our presentation of the results. In the following lines, we discuss the figures and all the points raised in your review.

**REVIEWER B:** *Because they are looking at very small events that they are picking out of the noise through a template matching, it would be a lot to expect that the events would be visually clear in the data. But even considering that I found the presentation of the data a bit puzzling, for example Figure 5. The stacks do seem to show something, but in the actual data (which are very small and hard to see), the red lines corresponding to the stack interval all have easily visible trends that are, in general, different from the long-term trend of the data. I honestly can't tell whether the data traces look like the stacks (maybe yes in Figure 5e), but if the deviations from the short-term trend are real signals then what are the changes in trend of the red lines (5b, 5e) relative to the long-term trend? It can't be a common-mode error, because the trend differences between the short term (red lines) and long term are different for every site. It appears from the figure that they are removing arbitrary (average) short-term trends and then stacking the residuals – what would the stacks look like if they did not include this arbitrary trend? The next question relates to panels c and f. These show what looks like a coherent pattern of displacement for some selected sites. But what do the displacements at the other sites look like? If I looked at the displacement field as a whole, would it just look like noise, and of what magnitude? Do events that do not match the stack show more or less zero displacement, or similar-sized displacements to those shown, or larger displacements? In short, I want to see at least one good example that is very clear that shows the signal being extracted from the original data.*

In the revised version of Figures 5 and 6 (a), we now present the correlation function used to detect the events (green lines), along with the weighted stack (black dots) and the corresponding model of the SSEs (red lines). We have changed event #7 by the #10 to showcase an SSE example occurring during the interseismic phase. In addition, we have extended the correlation functions, stacks and model to 90 days before (light blue) and after (light green) each detected event. By comparing these results, we confirm that our detections correspond to emerging signals picked up within geodetic noise.

We agree that the way we presented the time series in the previous version of the manuscript was not optimal ( $\sqrt{(E^2 + N^2)}$ ). Now, we show the North and East displacement time series (Figures 5 and 6, b and c) for all stations used in the weighted stack of Event # 12 (6 stations) and Event #10 (5 stations, and all the events in the Supporting Information). On top of each displacement time series, we plot a model

for the estimated magnitude for the SSEs (green lines), as well as the estimation of the displacement from the data (pink lines). For event #12 case, we observe stations AEDA and CRSC toward the west. Such displacements agree with the displacement generated by an SSE, which is the same case for event #10 case.

Upon examining these displacement fields on a map, we observe that the stations used to compute the correlation functions move the way we would expect them to move during an SSE (Figures 5 and 6 d, pink and green arrows), while stations located further away (black arrows) do not. We believe this suggests that signals detected by the method are unrelated to the common-mode. However, it is worth noting small discrepancies between the displacement observed in the data and the magnitudes predicted by the model. Our methodology interprets the results under the assumption that slip is centered at the node corresponding to the peak of the correlation function is originated, as illustrated in the updated Figures 5 and 6 e. These figures reveal that areas of positive correlation are widespread; nonetheless, we treat the origin of the SSEs as point sources. Drawing an analogy with earthquakes, our approach conceptualizes SSEs as static, point-like events rather than kinematic sources. As a result, there is a small impact in the magnitude estimation that is addressed by assessing their uncertainties, as well as we cannot capture potential slip migration, a point that goes beyond the scope of the present work.

We would like to thank Pr. Freymueller's comment regarding the trends observed in our study. In response, we have broadened the analysis period for stacking to 180 days and uniformly removed trends for all events using the initial 60 days of the time series. This adjustment, detailed in Figures 5 and the Supporting Material (Figures S33-S43), has been key in eliminating spurious trends and enhancing the clarity of the stack displacements. While some deviations in stack velocity remain for some events, the deviations we observed range between  $10^{-3}$  -  $10^{-1}$  mm/yr, as illustrated in Figure RB3. We trust this clarification addresses the concerns raised and we are thankful for Professor Freymueller's contribution towards refining the presentation of our findings.

**REVIEWER B:** *Lines 330-336 and Figure 6 (and S42). How is this scaling (slope) estimated? Figure 6 (and S42) shows a cloud of points. Certainly the slope of a line passing through those points is not constrained meaningfully by shape of the cloud. Yet somehow the authors derive a slope of  $3 \pm 0.01$ , an incredibly certain value. Figure S42 is entirely non-convincing in this regard; given the degree of misfit shown, I cannot see how they can justify such a microscopic uncertainty. Their slope estimate must be largely determined by some unstated assumption, presumably the intercept value at  $M_0=0$ , but maybe something else as it is never stated. Figure 6 shows a change in slope immediately to the right of their data points for the gray field labeled SUG. How do they know that there are not other breaks in slope somewhere to the left of their cloud of points? The assumptions that go into the estimate of scaling need to be stated much more clearly. What things have they assumed with certainty when deriving this extremely precise estimate of the slope, and are those things truly certain (or simply the models they have tested)?*

In addition to the need for a clearer explanation of the parameter estimation, we realized that we were incorrectly sampling the model space. This issue introduced minor uncertainties in the T scaling estimation, which, as Pr. Freymueller suggested, seemed unrealistic.

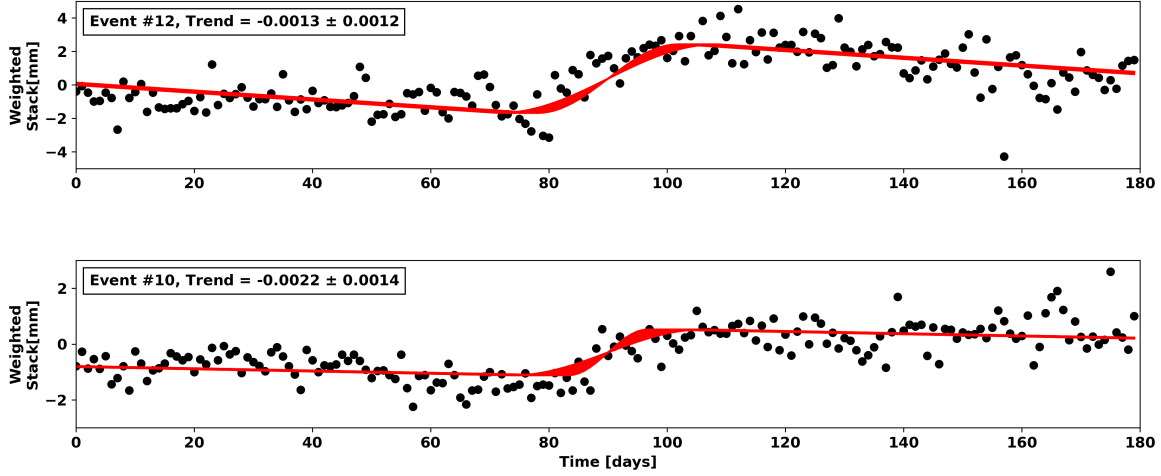


Figure RB3: Weighted Stack (black dots) and preferred SSE model (red lines) for Events #12 (a) and Event #7.

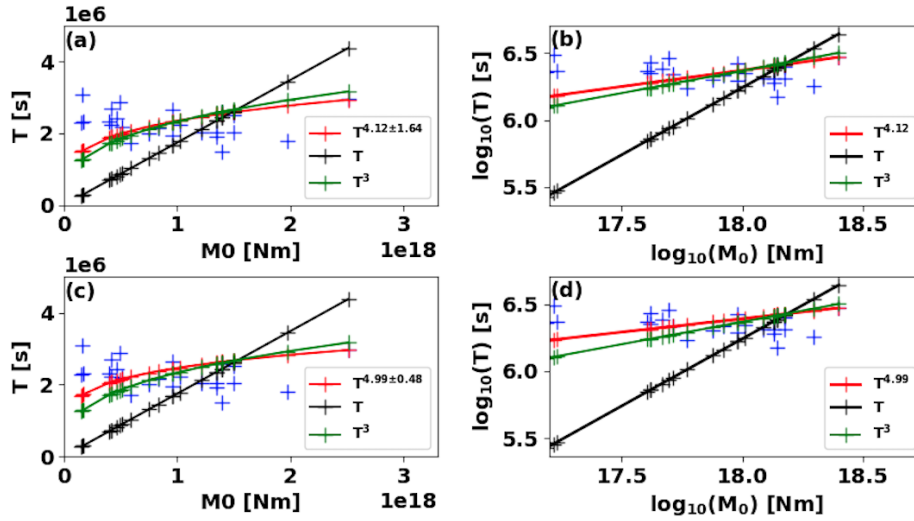


Figure RB4: (a) Moment-duration scaling estimated by using a curve fitting method (Virtanen et al., 2020) in Eq. 1, with  $T$  [s] and  $M_0$  [Nm]. (b) same as (a) in  $\log\log$  scale. The black lines represent a  $M \propto T$  scaling, while green ones are  $M \propto T^3$ , and red lines represent the inverted values  $M \propto T^{4.12 \pm 1.64}$ . (c) and (b), same as (a) and (b), but parameters are estimated using a Bayesian framework (Abril-Pla et al., 2023). Colors are the same as described above, but red lines are a  $M \propto T^{4.99 \pm 0.48}$  scaling, where the standard deviation represents 94% of a confidence interval.

We therefore now include a step-by-step explanation in the supporting information as follows:

We determine the moment-duration scaling following the approach of Michel et al. (2019). The moment-duration relation writes as,

$$\log_{10}(T) = \frac{1}{c} \log_{10}(M_0) + g, \quad (1)$$

where  $T$  is the event duration in seconds,  $M_0$  the moment magnitude in [Nm],  $c$  the temporal scaling factor, and  $g$  a constant. In order to estimate the scaling factor  $c$ , we use the curve fit function from the Scipy Python package (Virtanen et al., 2020) to fit Eq. 1 to our data, resulting in a moment-duration scaling of  $M \propto T^{4.12 \pm 1.64}$  (red curve, Figure RB4 a and b). We set bounds for  $c$  to  $[0.1, 100]$  and  $g$  to  $[-35, 1000]$ .

We also compare our detections with best fitting  $T$  and  $T^3$  scalings (black and green curves, Figure RB4 a and b). Despite the limitations of our method in resolving a large magnitude range, our results consistently suggest a scaling closer to  $T^3$  rather than  $T$ . This finding holds both in the time/magnitude space (Figure RB4 a) and the log-log space (Figure RB4 b).

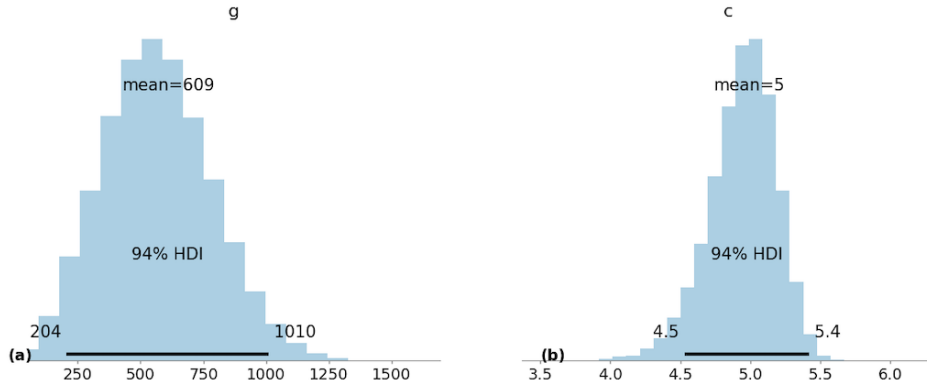


Figure RB5: PDF for estimated parameters  $g$  (a) and  $c$  (b) in Eq. 1, using a Bayesian framework. On top of each PDF, the mean parameter values are shown, whereas, at bottom, the 94% confidence intervals are indicated.

We then use the Python PyMC solver (Abril-Pla et al., 2023) to explore a broader solution space and provide an uncertainty analysis of the estimated parameters. We set priors as uniform distributions bounded by  $[0.1 - 100]$  for  $c$  and  $[-35, 1000]$  for  $g$ . We examine 5.000.000 models to estimate the posterior distribution, giving a mean value for  $c$  of  $4.99 \pm 0.48$  and  $g$  of  $609 \pm 400$ , both with a 94% confidence interval (Figure RB5). It is important to highlight that these results hold when categorizing the events as A (probables, Figures S47-S48) and B (possibles, Figures S49-S50).

Subsequently, we compare our results against published equations for scaling relationships. Gomberg et al. (2016) evaluates theoretical moment-duration scaling for spatially bounded and unbounded ruptures, whether slow or fast, considering the width of the region in which events occur ( $W_{max}$ ), their stress drop ( $\Delta\tau$ ) and their rupture velocity ( $V$ ).

For a rupture with unbounded growth, rupture time scales with moment as

$$\log(T) = \frac{1}{3} \log(M_0) - \frac{1}{3} \log(c\Delta\tau V^3), \text{ for } M_0 < c\Delta\tau W_{max}^3. \quad (2)$$

For a rupture with a bounded growth, rupture time scales with moment as

$$\log(T) = \log(M_0) - \log(c\Delta\tau W_{max}^3), \text{ for } M_0 > c\Delta\tau W_{max}^3, \quad (3)$$

where  $c$  is a constant ( $\frac{3\pi}{16}$ ), and  $M_0$  the seismic moment. To draw the slow bounded and unbounded regions in Figure 6 in the main text, we assume a  $\Delta\tau$  of 0.1 MPa, rupture velocities of 1 and 5 km/day, and a  $W_{max}$  of 30 km, a value inferred from geodetic and seismological observations (Chlieh et al., 2004; Comte et al., 2016). For the fast region case, we use  $\Delta\tau$  values of 0.2 and 0.5 MPa, ruptures velocities of 1-2 km/s, and the same above-mentioned  $W_{max}$ .

It is worth noting that there are many factors that could affect the scaling estimates of our events. The detected events cover a very limited range of magnitudes (5.4-6.2), with considerable standard deviations for their durations. This could have an important impact on the estimation of the moment-duration scaling (Ide and Beroza, 2023). In addition, our method does not allow us to detect propagating events. Therefore, our events seem to be located more in the unbounded, crack-like region, rather than the pulsed, bounded ones. Taking all these constraints into account, we find that the seismic moment of our events in the Peru-Chile subduction region appears to have similar source properties that those observed in other subduction zones (Ide and Beroza, 2023, and reference therein). In addition, we provide a new database of slow slip events that can be used in global studies on this subject—a topic beyond the scope of the present manuscript.

**REVIEWER B:** *Lines 424-432. This discussion completely ignores the uncertainty in the depths/locations of the events. First, what is that uncertainty, and second, is it small enough to justify the interpretations? Give the uncertainties in depths, including the depth range (and uncertainty) of the presence of lithospheric mantle. Many of the events are located right at the updip end of the inferred presence of lithospheric mantle. There is likely an uncertainty of at least 1-2 km in that depth, and quite possibly more, which could shift that boundary laterally by a considerable distance. Similarly, the location of the events (stars in Fig 9) likely have substantial uncertainties. I can't tell whether their interpretation is robust given the uncertainty in both the event locations and the underlying cross-section elements.*

We apologize for not being clear about the depth discussion and for not adequately addressing the associated uncertainties. We now include a description of the process by which we obtain the information shown in Figure 9 to the Supporting Information, as follows:

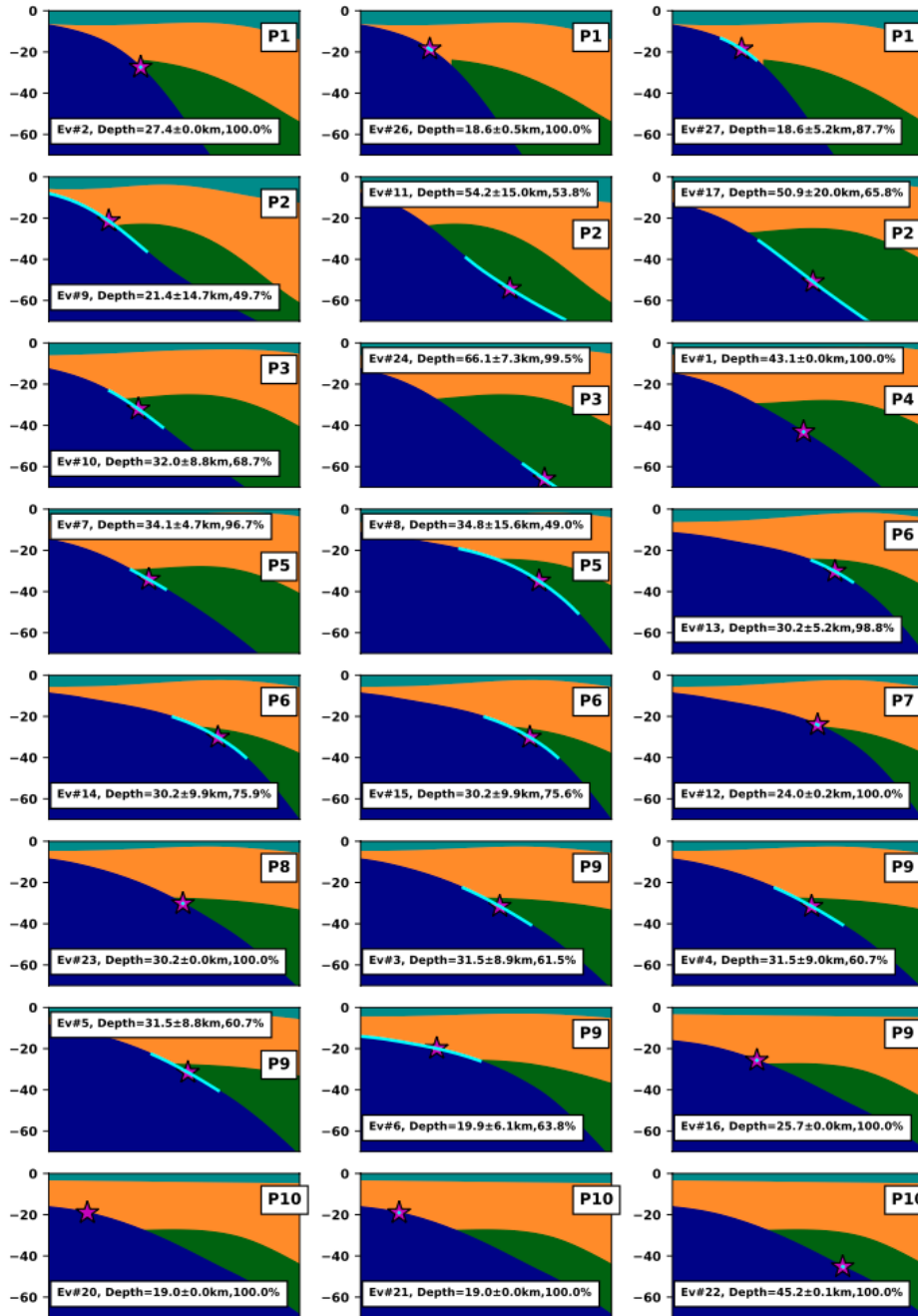


Figure RB6: Location of the event at depth. Colors indicate structure at depth (upper and lower crust, lithospheric mantle, asthenospheric wedge, and oceanic crust). White boxes indicate event IDs along each profile, depth, and their probability of being within the polygon used to perform the analysis.

We contrast our results with a 3D gravity model in the (Tassara and Echaurren, 2012) zone to compare our results with large tectonic structures and their possible relationship to fluids. We project the detected events onto trench perpendicular cross sections. We then project the uncertainties associated with these

detections on the cross sections. To consider an uncertainty analysis on the depth of our events, we employ a multivariate normal distribution  $\{\mathbf{x}\} = \mathcal{N}_2(\mu_{1e}, \sigma_{1e}^2)$ , assuming that the event location is normally distributed. Here,  $\mu_{1e}$  corresponds to the event location, while  $\sigma_{1e}$  is the covariance matrix of the location, which is based on the standard deviation of each event obtained during the synthetic analysis. We project these uncertainties on the megathrust and show the extent of the regions in which the detected event could be located (cyan lines in Figure RB6).

**REVIEWER B:** *Minor comments*

*Line 189. This is a highly asymmetric Gaussian distribution. Or else a substantially truncated one. A figure (supplemental OK) would help visualize this. It would seem to have a strong preference for zero, but it is hard to say what it looks like after re-normalization. Also, what sigma scales the width of the underlying distribution? That is never stated.*

We have included a figure in the Supporting Information (Figure RB7) depicting the mean coupling distribution, as well as the *a priori* and *a posteriori* probability density functions, for five nodes within the mesh (out of 289). Additionally, there was a typo in line 230, where ‘5’ should be replaced with ‘0.5.’ We have made the necessary changes to the main text. We have made the following changes in the main text.

The *a priori* PDF describes our knowledge of coupling along the megathrust before collecting geodetic data. We define the *a priori* PDF of coupling as

$$X \sim \begin{cases} \mathcal{N}(\mu_c, \sigma_c^2) & \text{if } -0.1 \leq X \leq 1.1 \\ 0 & \text{otherwise} \end{cases} \quad (4)$$

where  $\mu_c$  and  $\sigma_c$  are the mean and standard deviation of a normal distribution. We select the bounds of [-0.1, 1.1] to ensure an accurate sampling for the full range of coupling values between 0 and 1 (Dal Zilio et al., 2020; Jolivet et al., 2020). We know the megathrust is decoupled below 60 km depth from geodetic (Chlieh et al., 2004; Béjar-Pizarro et al., 2013; Jolivet et al., 2020) and seismological evidence (Comte et al., 2016). Thus, we apply an *a priori* condition based on the depth of each node. If a node is deeper than 60 km, the *a priori* mean ( $\mu_c$ ) is set to 0 and the standard deviation ( $\sigma_c$ ) to 0.1. In cases where a node is shallower than 60 km, we assign an *a priori* mean ( $\mu_c$ ) of 0.5 and a standard deviation ( $\sigma_c$ ) of 0.5.

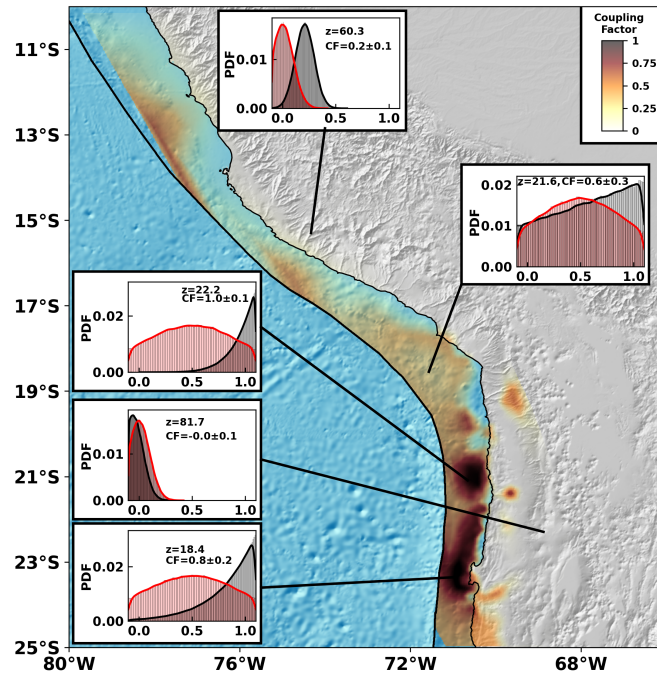


Figure RB7: Background color from white to dark through yellow and red is the mean coupling distribution. Dark red areas (coupling factor  $\sim 1$ ) are locked, while transparent areas (coupling factor  $\sim 0$ ) slip aseismically at a rate equal to the plate convergence rate. Five *a priori* (red) and *a posteriori* (gray) probability density functions (PDF) are shown for five nodes along the slab mesh.

**REVIEWER B:** Lines 192-193. The units for the *a priori* PDF of coupling are not clear given the values provided. What does an *a priori* standard deviation of 5 mean on a quantity that varies nominally from 0-1 (with values  $\neq 0$  indicating slip), and again, how does this look if truncated?

We address this answer in the previous point.

**REVIEWER B:** Line 342. What is “a distribution coupling”? Certainly the English is wrong here, but it is hard to guess what they really mean.

We apologize for the error. We meant ‘coupling distribution’ instead of ‘distribution coupling’. We change the main text accordingly.

**REVIEWER B:** Figure 7. What exactly are these probabilities of? Be more specific about exactly what quantity this PDF refers to. For example, I think panels a-c are meant to indicate that randomly located events would have a tendency to be located in areas of zero coupling, while the events are located

*differently with respect to the interseismic coupling. But the steps between taking 24 sample locations (each with uncertainty!) and deriving a continuous curve are not stated, and not clear at all to me. I could see a histogram representation, but how do you get a smooth curve? And where do the 1000 coupling models come from? How do these models relate to the model shown in Figure 3. Clearly specify your process here. Panels d-g are even less clear. What is “the PDF of depth of 24 random events”? (Same for the located events). Each event surely has a PDF for it’s own depth – is this simply all of those multiplied together and renormalized? Or something else? Please present something that is clear for the reader to understand, and explain what you did to get it. Maybe show an example that illustrates how this is derived? And why do you have random events at 100-150 km depth? That seems rather pointless, as it is hard to believe that events would be down there. It raises the question of how the random events were selected/generated? Without that tail on the random events, I am not sure that the depth distribution of the random events would look much different than that of the located events.*

We have added a step-by-step procedure on how we obtained the values shown in Figure 7 in the main manuscript. Such a procedure is described in the Supporting Information as follows.

#### **Text S5. PDF for coupling, depth, and Vp/Vs ratio**

**PDF of coupling.** We perform a statistical analysis to compare our coupling distribution with the detected events (see Figure 7a, b, c). This analysis involves comparing random values with those associated with our detected events. Our coupling model, illustrated in Figure 3 (main text), represents an average derived from 250,000 models. Initially, we selected 1000 random coupling models for the entire region, randomly sampling 24 points for each model (i.e. the number of detected events) to build the PDF of coupling at the location of SSEs if those were randomly distributed (see Figure RB8a). We then compute the probability density function (PDF) of coupling at the location of our detected events. We approximate both PDFs using a Kernel Density Estimate (KDE). The analysis reveals that random values exhibit a distribution with a mean and standard deviation of  $0.33 \pm 0.35$  (as shown by the gray line in Figure a). In contrast, for our detected events, we obtained  $\mu \pm \sigma = 0.44 \pm 0.32$  (as indicated by the dark green line in Figure b).

Given the distinct resolution over the Peruvian and Chilean regions, we conduct a separate analysis for each region (Peru, latitude  $>19^\circ\text{S}$ , and Chile, latitude  $\leq 19^\circ\text{S}$ ). In Peru, randomly sampled events yield coupling values with a mean and standard deviation of  $0.2 \pm 0.26$  (gray line in Figure RB8, c), while our detections exhibit values of  $\mu \pm \sigma = 0.24 \pm 0.2$  (blue line in Figure RB8, d). For Chile, randomly sampled values are  $\mu \pm \sigma = 0.37 \pm 0.36$  (gray line in Figure RB8, e), whereas our detections show values of  $\mu \pm \sigma = 0.56 \pm 0.31$  (magenta line in Figure RB8, f).

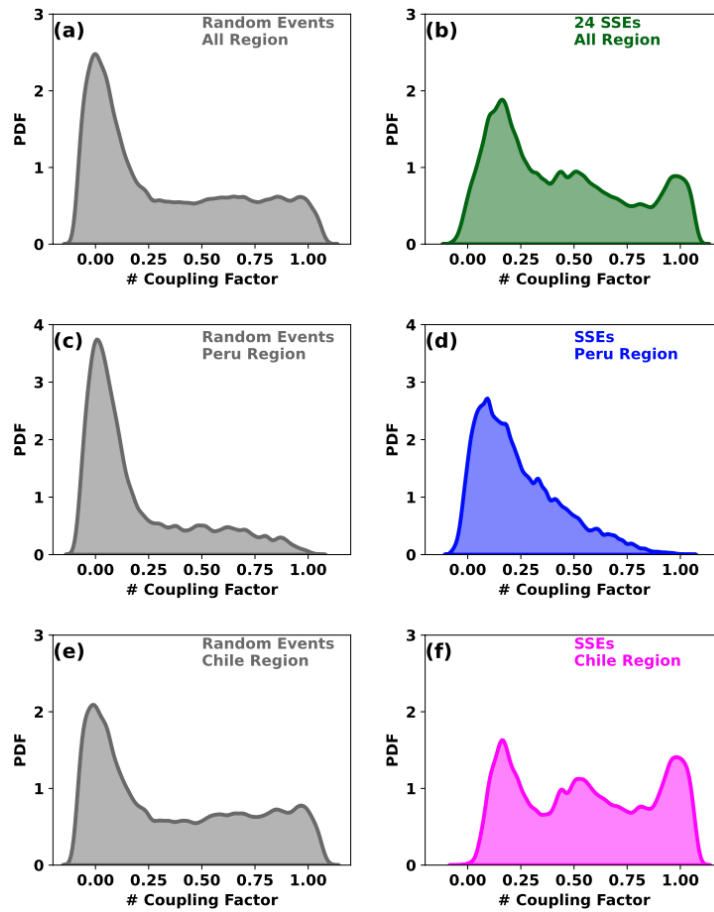


Figure RB8: Probability Density Function (PDF) of coupling for our 24 detected events/random picks. (a) Random points PDF for the entire region, and the dark gray line denotes the Kernel Density Estimation. (b) same as (a), but for the location of our 24 detected events. (c), (d) and, (e), (f) are the same as (a) and (b), but in the Peruvian and Chilean regions.

Although the PDF are not definitive on that point, detected events in Chile tend to cluster in areas where coupling is average. While the results suggest a similar trend in the Peruvian region, the relationship is less clear. This potential disparity may stem from differences in data density between the regions (GNSS stations and InSAR in Chile, and just GNSS in Peru) and the sparse distribution of GNSS stations in Peru. It is important to highlight that these results hold when categorizing the events as A (probable, Figure S56 a, b, and c) and B (possible, Figure S57 a, b and c).

**PDF of Depths.** We perform a similar statistical analysis on the depth distribution of our detected events. To eliminate the possibility that the localization and clustering of our events result from chance, we compare our detections with events randomly distributed along the megathrust. Initially, we generate 10,000 sets of 24 random events to build the PDF of depth of these random picks(Figure RB9a). For detected events, we generate 10,000 locations for each detection drawn from a multivariate normal distribution

$\mathbf{x} = \mathcal{N}_2(\mu_{le}, \sigma_{le}^2)$ , assuming a normal error distribution for the event location. Here,  $\mu_{le}$  is the event location (longitude and latitude), while  $\sigma_{le}$  is the standard deviation drawn from the covariance matrix of the synthetic event analysis.

Subsequently, for a detailed analysis, we computed PDFs and KDE of random values from depths shallower than 60 km. This analysis relies on the fact that our events tend to occur at these depths. We repeat the same procedure used for the entire region, as well as the Chilean and Peruvian regions, for randomly distributed events (Figure RB9b, e, h). Our results reveal distinct distributions between random events and actual locations. Random distributions exhibit either a highly flattened normal distribution across all depths or a nearly uniform distribution for depths  $\leq 60$  km. In contrast, our detected events tend to cluster at depths corresponding to the transition zone (Chlieh et al., 2004; Comte et al., 2016). It is important to highlight that these results hold when categorizing the events as A (probable, Figure S56 d, e, and f) and B (possible, Figure S56 d, e, and f).

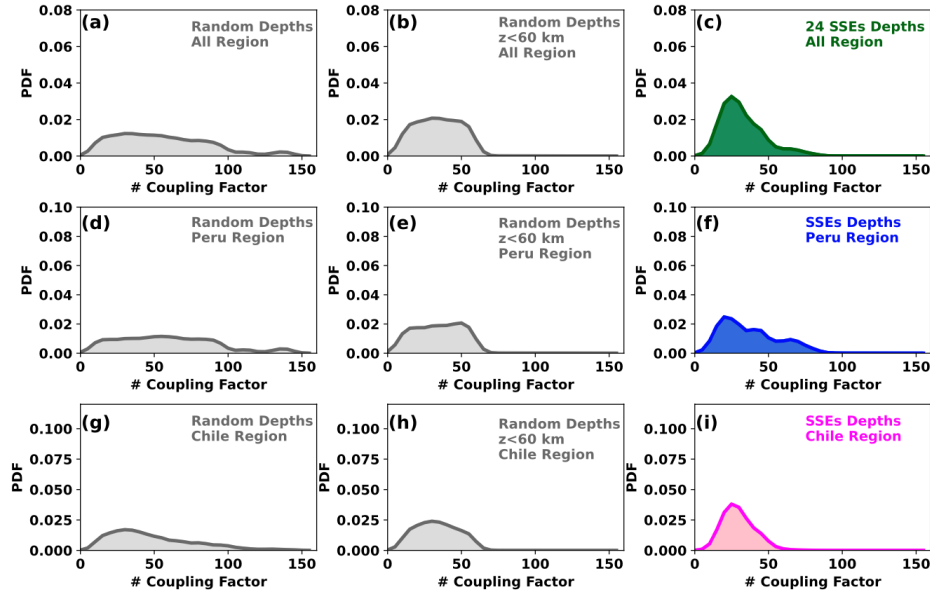


Figure RB9: Depth Probability Density Functions (PDF) for 24 detected events/random picks. (a) Random picks PDF for the entire region, with the dark gray line representing the Kernel Density Estimation (KDE). (b) same as (a), but for depths shallower than 60km. (c) same as (a), but for the depths of our detected events. (d), (e), and (f) same as (a), (b), and (c) for the Peruvian regions, while (g), (h), (i) for the Chilean regions.

**PDF of  $V_p/V_s$  ratio.** We compare our results with the  $V_p/V_s$  ratio to explore a potential relationship with fluids. Fluids, a factor influencing the underlying physics of slow events (Jolivet and Frank, 2020, and references therein), can be inferred from estimates of  $V_p/V_s$  ratio (Comte et al., 2016, and references therein). Here, we use the  $V_p/V_s$  model by Comte et al. (2016) for northern Chile. From this model, we

can derive a Vp/Vs ratio only for 17 of our events. First, we randomly sample 17 points in the Vp/Vs model 1000 times to build the PDF of Vp/Vs (Figure RB10a, gray line). Second, we generate 1000 synthesized events for each detection using a multivariate normal distribution  $\mathbf{x} = \mathcal{N}_2(\mu_{1e}, \sigma_{1e}^2)$ , assuming a normally distributed event location. Here,  $\mu_{1e}$  signifies the event location (longitude and latitude), and  $\sigma_{1e}$  is the covariance matrix based on the standard deviation of each event obtained during the synthesized event analysis. It is important to highlight that these results hold when categorizing the events as A (probable, Figure S56 g) and B (possible, Figure S56 g).

These results suggest that the observed distributions are not significantly distinct. One plausible explanation is that our events may occur in regions devoid of a permanent fluid source, as indicated by the Vp/Vs ratio mapping. However, this does not preclude the possibility of rapid fluid migrations contributing to event generation (Contreras-Reyes et al., 2021; Bouchon et al., 2023) or an aseismic response induced by pore pressure waves (Cruz-Atienza et al., 2018). Both hypotheses require further investigation and are beyond the scope of this manuscript.

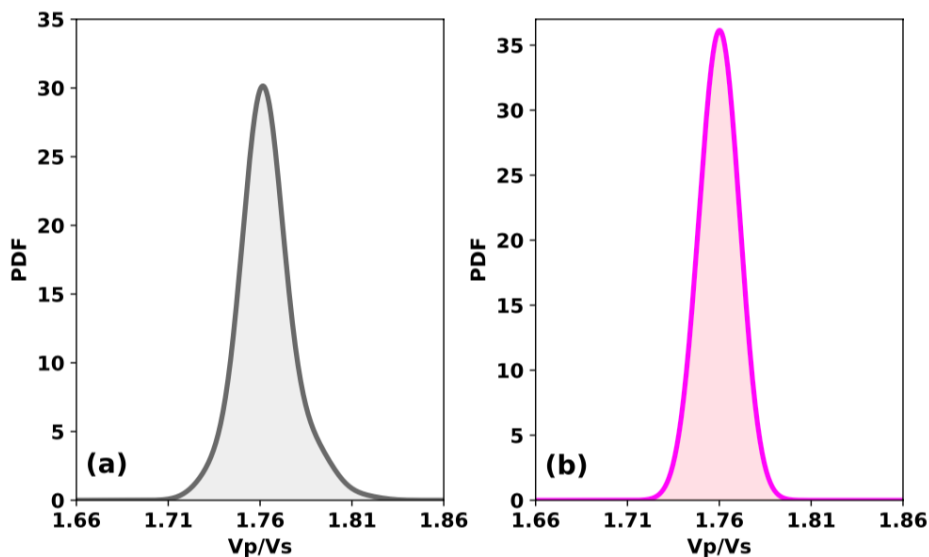


Figure RB10: Vp/Vs ratio Probability Density Functions (PDF) and KDE for random picks (a) and 17 detected events (b).

## References

Abril-Pla, O., Andreani, V., Carroll, C., Dong, L., Fannesbeck, C. J., Kochurov, M., Kumar, R., Lao, J., Luhmann, C. C., Martin, O. A., Osthege, M., Vieira, R., Wiecki, T., and Zinkov, R. PyMC: a modern, and comprehensive probabilistic programming framework in Python. *PeerJ Computer Science*, 9:e1516, 2023. doi: 10.7717/peerj-cs.1516.

- Béjar-Pizarro, M., Socquet, A., Armijo, R., Carrizo, D., Genrich, J., and Simons, M. Andean structural control on interseismic coupling in the North Chile subduction zone. *Nature Geoscience*, 6(6):462–467, 6 2013. doi: 10.1038/ngeo1802.
- Bouchon, M., Marsan, D., Jara, J., Socquet, A., Campillo, M., and Perfettini, H. Suspected Deep Interaction and Triggering Between Giant Earthquakes in the Chilean Subduction Zone. *Geophysical Research Letters*, 45(11): 5454–5460, 6 2018. doi: 10.1029/2018GL078350.
- Bouchon, M., Guillot, S., Marsan, D., Socquet, A., Jara, J., and Renard, F. Observation of a Synchronicity between Shallow and Deep Seismic Activities during the Foreshock Crisis Preceding the Iquique Megathrust Earthquake. *Seismica*, 2(2), 10 2023. doi: 10.26443/seismica.v2i2.849.
- Boudin, F., Bernard, P., Meneses, G., Vigny, C., Olcay, M., Tassara, C., Boy, J. P., Aissaoui, E., Métois, M., Satriano, C., Esnault, M.-F., Necessian, A., Vallée, M., Vilotte, J.-P., and Brunet, C. Slow slip events precursory to the 2014 Iquique Earthquake, revisited with long-base tilt and GPS records. *Geophysical Journal International*, 228(3):2092–2121, 2021. doi: 10.1093/gji/ggab425.
- Chlieh, M., De Chabalier, J. B., Ruegg, J. C., Armijo, R., Dmowska, R., Campos, J., and Feigl, K. L. Crustal deformation and fault slip during the seismic cycle in the North Chile subduction zone, from GPS and InSAR observations. *Geophysical Journal International*, 158(2):695–711, 2004. doi: 10.1111/j.1365-246X.2004.02326.x.
- Comte, D., Carrizo, D., Roecker, S., Ortega-Culaciati, F., and Peyrat, S. Three-dimensional elastic wave speeds in the northern Chile subduction zone: Variations in hydration in the supraslab mantle. *Geophysical Journal International*, 207(2):1080–1105, 2016. doi: 10.1093/gji/ggw318.
- Contreras-Reyes, E., Díaz, D., Bello-González, J. P., Slezak, K., Potin, B., Comte, D., Maksymowicz, A., Ruiz, J. A., Osses, A., and Ruiz, S. Subduction zone fluids and arc magmas conducted by lithospheric deformed regions beneath the central Andes. *Scientific Reports*, 11(1):1–12, 2021. doi: 10.1038/s41598-021-02430-9.
- Cruz-Atienza, V. M., Villafuerte, C., and Bhat, H. S. Rapid tremor migration and pore-pressure waves in subduction zones. *Nature Communications*, 9(1), 2018. doi: 10.1038/s41467-018-05150-3.
- Dal Zilio, L., Jolivet, R., and van Dinther, Y. Segmentation of the Main Himalayan Thrust Illuminated by Bayesian Inference of Interseismic Coupling. *Geophysical Research Letters*, 47(4):1–10, 2020. doi: 10.1029/2019GL086424.
- Gomberg, J., Wech, A., Creager, K., Obara, K., and Agnew, D. Reconsidering earthquake scaling. *Geophysical Research Letters*, 43(12):6243–6251, 6 2016. doi: 10.1002/2016GL069967.
- Ide, S. and Beroza, G. C. Slow earthquake scaling reconsidered as a boundary between distinct modes of rupture propagation. *Proceedings of the National Academy of Sciences*, 120(32):2017, 8 2023. doi: 10.1073/pnas.2222102120.
- Jara, J., Socquet, A., Marsan, D., and Bouchon, M. Long-Term Interactions Between Intermediate Depth and Shallow Seismicity in North Chile Subduction Zone. *Geophysical Research Letters*, 44(18):9283–9292, 9 2017. doi: 10.1002/2017GL075029.
- Jolivet, R. and Frank, W. B. The Transient and Intermittent Nature of Slow Slip. *AGU Advances*, 1(1), 2020. doi: 10.1029/2019av000126.

- Jolivet, R., Simons, M., Duputel, Z., Olive, J. A., Bhat, H. S., and Bletery, Q. Interseismic Loading of Subduction Megathrust Drives Long-Term Uplift in Northern Chile. *Geophysical Research Letters*, 47(8):1–11, 2020. doi: 10.1029/2019GL085377.
- Melnick, D., Moreno, M., Quinteros, J., Baez, J. C., Deng, Z., Li, S., and Oncken, O. The super-interseismic phase of the megathrust earthquake cycle in Chile. *Geophysical Research Letters*, 44(2):784–791, 2017. doi: 10.1002/2016gl071845.
- Michel, S., Gualandi, A., and Avouac, J.-P. Similar scaling laws for earthquakes and Cascadia slow-slip events. *Nature*, 574(7779):522–526, 10 2019. doi: 10.1038/s41586-019-1673-6.
- Rousset, B., Campillo, M., Lasserre, C., Frank, W. B., Cotte, N., Walpersdorf, A., Socquet, A., and Kostoglodov, V. A geodetic matched filter search for slow slip with application to the Mexico subduction zone. *Journal of Geophysical Research: Solid Earth*, 122(12):498–10, 12 2017. doi: 10.1002/2017JB014448.
- Ruiz, S., Klein, E., del Campo, F., Rivera, E., Poli, P., Metois, M., Christophe, V., Baez, J. C., Vargas, G., Leyton, F., Madariaga, R., and Fleitout, L. The Seismic Sequence of the 16 September 2015 Mw 8.3 Illapel, Chile, Earthquake. *Seismological Research Letters*, 87(4):789–799, 7 2016. doi: 10.1785/0220150281.
- Ruiz, S., Moreno, M., Melnick, D., del Campo, F., Poli, P., Baez, J. C., Leyton, F., and Madariaga, R. Reawakening of large earthquakes in south central Chile: The 2016 Mw7.6 Chiloé event. *Geophysical Research Letters*, 44(13):6633–6640, 7 2017. doi: 10.1002/2017GL074133.
- Tassara, A. and Echaurren, A. Anatomy of the Andean subduction zone: three-dimensional density model upgraded and compared against global-scale models. *Geophysical Journal International*, 189(1):161–168, 4 2012. doi: 10.1111/j.1365-246X.2012.05397.x.
- Virtanen, P., Gommers, R., Oliphant, T. E., Haberland, M., Reddy, T., Cournapeau, D., Burovski, E., Peterson, P., Weckesser, W., Bright, J., van der Walt, S. J., Brett, M., Wilson, J., Millman, K. J., Mayorov, N., Nelson, A. R. J., Jones, E., Kern, R., Larson, E., Carey, C. J., Polat, I., Feng, Y., Moore, E. W., VanderPlas, J., Laxalde, D., Perktold, J., Cimrman, R., Henriksen, I., Quintero, E. A., Harris, C. R., Archibald, A. M., Ribeiro, A. H., Pedregosa, F., van Mulbregt, P., Vijaykumar, A., Bardelli, A. P., Rothberg, A., Hilboll, A., Kloeckner, A., Scopatz, A., Lee, A., Rokem, A., Woods, C. N., Fulton, C., Masson, C., Häggström, C., Fitzgerald, C., Nicholson, D. A., Hagen, D. R., Pasechnik, D. V., Olivetti, E., Martin, E., Wieser, E., Silva, F., Lenders, F., Wilhelm, F., Young, G., Price, G. A., Ingold, G.-L., Allen, G. E., Lee, G. R., Audren, H., Probst, I., Dietrich, J. P., Silterra, J., Webber, J. T., Slavič, J., Nothman, J., Buchner, J., Kulick, J., Schönberger, J. L., de Miranda Cardoso, J. V., Reimer, J., Harrington, J., Rodríguez, J. L. C., Nunez-Iglesias, J., Kuczynski, J., Tritz, K., Thoma, M., Newville, M., Kümmerer, M., Bolingbroke, M., Tartre, M., Pak, M., Smith, N. J., Nowaczyk, N., Shebanov, N., Pavlyk, O., Brodtkorb, P. A., Lee, P., McGibbon, R. T., Feldbauer, R., Lewis, S., Tygier, S., Sievert, S., Vigna, S., Peterson, S., More, S., Pudlik, T., Oshima, T., Pingel, T. J., Robitaille, T. P., Spura, T., Jones, T. R., Cera, T., Leslie, T., Zito, T., Krauss, T., Upadhyay, U., Halchenko, Y. O., and Vázquez-Baeza, Y. SciPy 1.0: fundamental algorithms for scientific computing in Python. *Nature Methods*, 17(3):261–272, 3 2020. doi: 10.1038/s41592-019-0686-2.